Toward regional-scale modeling using the two-way nested global model TM5

Peters, W.; Krol, M. C.; Dlugokencky, E. J.; Dentener, F. J.; Bergamaschi, P.; Dutton, G.; Velthoven, P. V.; Miller, J. B.; Bruhwiler, L.; Tans, P. P.

Published in:
Journal of geophysical research-Atmospheres

DOI:
10.1029/2004JD005020

Publication date:
2004

Toward regional-scale modeling using the two-way nested global model TM5: Characterization of transport using SF_6

W. Peters,[1,2] M. C. Krol,[3] E. J. Dlugokencky,[1] F. J. Dentener,[4] P. Bergamaschi,[4] G. Dutton,[1,2] P. v. Velthoven,[5] J. B. Miller,[1,2] L. Bruhwiler,[1] and P. P. Tans[1]

Received 14 May 2004; revised 26 July 2004; accepted 23 August 2004; published 12 October 2004.

[1] We present an evaluation of transport of sulfur hexafluoride (SF_6) in the two-way nested chemistry-transport model "Tracer Model 5" (TM5). Modeled SF_6 values for January 2000 to November 2003 are compared with NOAA CMDL observations. This includes new high-frequency SF_6 observations, frequent vertical profiles, and weekly flask data from more than 60 sites around the globe. This constitutes the most extensive set of SF_6 observations used in transport model evaluation to date. We find that TM5 captures temporal variability on all timescales well, including the relatively large SF_6 signals on synoptic scales (2–5 days). The model overestimates the meridional gradient of SF_6 by 19%, similar to previously used transport models. Vertical profiles are reproduced to within the standard error of the observations, and do not reveal large biases. An important area for future improvements is the mixing of the planetary boundary layer which is currently too slow, leading to modeled SF_6 mixing ratios that are too large over the continents. Increasing the horizontal resolution over North America from $6\times4^\circ$, to $3\times2^\circ$, to even $1\times1^\circ$ (lon×lat) does not affect the simulated global scale SF_6 distribution and potentially minimizes representation errors for continental sites. These results are highly relevant for future CO_2 flux estimates with TM5, which will be briefly discussed. *INDEX TERMS:* 0368 Atmospheric Composition and Structure: Troposphere—constituent transport and chemistry; 1610 Global Change: Atmosphere (0315, 0325); 0322 Atmospheric Composition and Structure: Constituent sources and sinks; 3210 Mathematical Geophysics: Modeling; *KEYWORDS:* regional inversions, SF_6, transport modeling

Citation: Peters, W., M. C. Krol, E. J. Dlugokencky, F. J. Dentener, P. Bergamaschi, G. Dutton, P. v. Velthoven, J. B. Miller, L. Bruhwiler, and P. P. Tans (2004), Toward regional-scale modeling using the two-way nested global model TM5: Characterization of transport using SF_6, *J. Geophys. Res.*, *109*, D19314, doi:10.1029/2004JD005020.

1. Introduction

[2] Atmospheric transport models play an important role in interpreting observations in the atmosphere. They relate measurements of aerosols and trace gases to their source locations, allowing us to estimate the contribution of different processes and different geographical regions to their budgets. For long-lived trace gases such as carbon dioxide (CO_2), transport models usually span the global domain since sources or sinks in the Northern Hemisphere (NH) can influence measurements in remote Southern Hemisphere (SH) locations, and vice versa. However, both researchers and policy makers want to know trace gas budgets on regional and smaller spatial scales. Such smaller scales are currently not well represented in global models, partly because the horizontal resolution of such models is insufficient.

[3] One way to work around this scale problem is to "nest" a regional model within a global model, transferring information from larger to smaller scales through fixed boundary conditions [*Taghavi et al.*, 2003; *Tang*, 2002; *Jonson et al.*, 2001]. Problems in this approach include the loss of information when transport across the nested model's domain occurs, and inconsistencies in transport due to the different resolutions (often even different models) being employed in separate calculations. In an approach that circumvents these issues, a finer grid is nested within a global model "online", i.e., with two-way transport of information in a single model run. The newly completed Tracer Model 5 (TM5) takes this approach [*Krol et al.*, 2004].

[1]Climate Monitoring and Diagnostics Laboratory, NOAA, Boulder, Colorado, USA.
[2]Cooperative Institute for Research in Environmental Sciences (CIRES), Boulder, Colorado, USA.
[3]Institute for Marine and Atmospheric Research Utrecht (IMAU), Utrecht, Netherlands.
[4]Joint Research Centre (JRC), Ispra, Italy.
[5]Royal Netherlands Meteorological Institute (KNMI), De Bilt, Netherlands.

0148-0227/04/2004JD005020

[4] TM5 will be used in a wide range of applications, which includes aerosol modeling, stratospheric chemistry simulations, hydroxyl-radical trend estimates [*Krol et al.*, 2003], assimilation of satellite data, and regional greenhouse gas flux estimates [*Bergamaschi et al.*, 2003]. The latter will be an important part of the North American Carbon Program (NACP, [*Wofsy and Harriss*, 2002]), in which TM5 will be used to derive fluxes of carbon-dioxide (CO_2) over the North American continent on a relatively fine scale ($\sim$70 km$\times$100 km). This is done through an 'inversion', in which observations from the NOAA's Climate Monitoring and Diagnostics Laboratory (NOAA CMDL) cooperative air sampling network are combined with transport from TM5 to produce global flux estimates that are optimally consistent with observations [see, e.g., *Tans et al.*, 1990; *Enting and Mansbridge*, 1989; *Ciais et al.*, 1995; *Fan et al.*, 1998; *Bousquet et al.*, 2000; *Gurney et al.*, 2002]. An important step before using TM5 for such purposes is to identify errors and biases in the simulated transport. Detailed knowledge of the model's transport characteristics is instrumental not only in interpreting atmospheric observations, but also in properly evaluating trace gas budgets and flux estimates calculated with TM5.

[5] One of the trace gases used to evaluate the simulated transport is sulfur hexafluoride (SF_6). It is an anthropogenic tracer released predominantly from high voltage electrical transformers where it is used as a spark quencher. SF_6 emissions do not vary seasonally [*Maiss and Brenninkmeijer*, 1998], and its atmospheric abundance has increased at an average rate of 0.20 pmol mol^{-1} yr^{-1}, (abbreviated ppt/yr) over the past decade. It has an atmospheric lifetime of $\sim$3000 years [*Ravishankara et al.*, 1993], and the magnitude and distribution of its sources are relatively well known. The global total source strength can be estimated to within 25% from bottom-up estimates [*Olivier and Berdowski*, 2001], with uncertainties on individual countries as large as 50–100%. This makes SF_6 an excellent tracer for atmospheric transport on timescales of weeks to years. SF_6 is measured from sites in NOAA CMDL's cooperative air sampling network. These observations allows us to estimate global SF_6 emissions to within 4% (assuming no drift in our calibration scale over time).

[6] SF_6 was used previously to study tracer transport [*Levin and Hesshaimer*, 1996], most recently in the Transport Model Intercomparison (TransCom) project [*Denning et al.*, 1999]. The second phase of TransCom aimed to characterize the transport behavior of eleven different transport models and quantify simulated differences with SF_6 observations, as well as inter-model differences. The TransCom II results focused on meridional and longitudinal gradients of SF_6. Models that were able to simulate SF_6 observations at marine boundary layer (MBL) sites well tended to perform poorly at continental sites, and vice versa, effectively dividing the eleven models into two families. The family each model fell into was determined by the amount of vertical mixing introduced through the subgrid-scale parameterizations of convection and vertical diffusion; models with vigorous mixing tended to do well for continental sites but underestimated surface SF_6 in the MBL, while more "trapping" models overestimated continental surface SF_6 and did well for MBL sites. Regular vertical profile measurements of SF_6 were not available at the time to verify either one of these families.

[7] Since the completion of TransCom II, the number of SF_6 observations has increased significantly. In addition to many more measurements from previously existing locations, five NOAA CMDL sites presented in this work now include vertical profiles up to $\sim$8 km altitude. The number of surface sites used here is about twice that of TransCom II and allows us to study transport in TM5 in three dimensions, on timescales down to weeks.

[8] In this work, we set out to answer the following questions: (1) How well does the new TM5 model simulate transport to NOAA CMDL sites, and what errors or biases are present? (2) What is the influence of TM5's two-way nested transport approach on simulated SF_6? and (3) Given the SF_6 results presented, what possible limitations and biases can we expect when we move to CO_2 inversions?

[9] To answer these questions we will start with a comparison of global scale features in SF_6 such as the meridional and so-called land-sea gradients (Sections 3 and 4). This is followed in Section 5 by a comparison of vertical profiles of SF_6 from several locations around the North American continent. In Section 6 we will discuss shortcomings in the modeled vertical mixing. Section 7 will shift focus to more regional features by investigating seasonal and daily time series for a number of continental sites, as well as sites in the marine boundary layer (MBL). Also, results with several layers of two-way grid-nesting will be introduced to see the effect of increased horizontal resolution on the simulated concentrations (Section 8). Finally, we will tie the SF_6 results to CO_2 in Section 9, and revisit the TransCom II results of *Denning et al.* [1999] to place our model in a suite of similar transport models that are frequently used for greenhouse gas flux estimates.

2. Method

2.1. SF_6 Measurements

[10] SF_6 data are from surface air samples collected as part of the CMDL Cooperative Air Sampling Network and from vertical profiles collected with a two-component portable sampling package. Surface samples are collected in duplicate, approximately weekly, from a globally distributed network of background air sampling sites [*Dlugokencky et al.*, 1994] that is shown in Figure 1. Vertical profiles are determined from samples collected using flask and compressor packages built into suitcases for portability. These packages are used on small, inexpensive turboprop aircraft to altitudes up to $\sim$7.6 km. No modification to the aircraft is necessary except for installation of a clean air inlet. Sampling frequency at each site varies from weekly to monthly. The flask packages contain 17 or 20 borosilicate glass flasks and a microprocessor to control flask valves. Flasks are cylindrical in shape, $\sim$1 L volume, and have glass-piston, Teflon-O-ring sealed stopcocks on each end. Materials used in these flasks are identical to those used in the surface network. Custom-built actuators, controlled by the microprocessor, are used to open and close stopcocks. The compressor package contains two compressors connected in series and batteries. During sampling, flask and compressor packages are connected by cables to transfer power and instructions from the micro

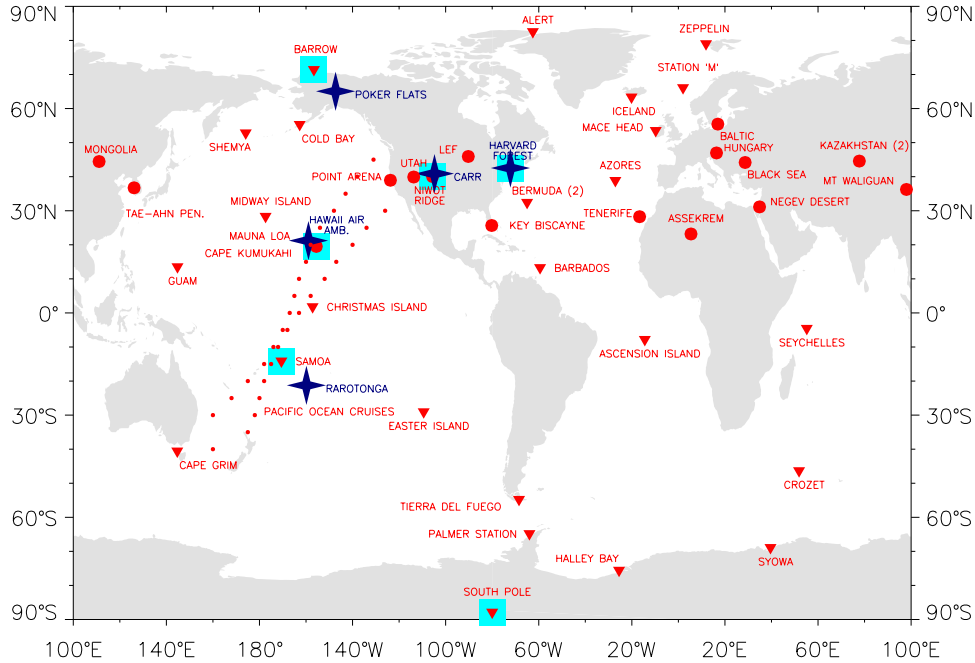

Figure 1. Map showing sites used in this study. Triangles denote 'marine boundary layer' sites; they are used to construct meridional gradients. Stars denote locations with vertical profiles of SF_6; squares are sites with high frequency SF_6 measurements.

processor, and tubing to get air from the compressors to the flasks. At each altitude, 10 L of ambient air is flushed through a flask, then it is pressurized to 0.28 MPa. The entire flask package is returned to Boulder for trace gas analyses, while the compressor package remains at the sampling site and its batteries are recharged.

[11] SF_6 dry-air mole fractions are determined at NOAA CMDL in Boulder, Colorado, USA by gas chromatography with electron capture detection (ECD) (for details, see *Geller et al.* [1997]). The ECD response to SF_6 is calibrated against the CMDL 2000 (gravimetrically-prepared) standard scale [*King and Schnell*, 2002]. Each aliquot of sample is bracketed by aliquots of natural air from a reference cylinder; repeatability of the analytical system is 0.04 ppt, determined as one standard deviation of multiple measurements of air from a cylinder containing natural air. In addition to SF_6, samples are also analyzed for CO_4 CO_2 CO, H_2, N_2O, and $\delta^{13}C$ and $\delta^{18}O$ in CO_2.

[12] Five NOAA field sites (SPO, SMO, MLO, NWR, BRW) and one in Harvard Forest (HFM) are equipped with GCs that sample air from a 10m tower once an hour. Each in situ GC is fitted with four electron capture detectors and packed or capillary columns tuned to measure a variety of trace gases including SF_6. To separate SF_6, two 1.59 mm o.d. packed columns of Porapak Q are used (2m pre-column and 3m main column) and are thermally controlled at 60°C. The air samples are compared to two on-site calibrated reference tanks that are sampled once every two hours. SF_6 estimated precisions range from 0.03 to 0.05 ppt.

2.2. Model Description

[13] TM5 is the next evolution of the widely used Tracer Model (TM) series that started in the late-1980s with TM2 [*Heimann and Keeling*, 1989; *Heimann*, 1995], later to be followed by several versions of TM3 [*Houweling et al.*, 1998; *Rodenbeck et al.*, 2003; *Dentener et al.*, 2003]. TM5 is based on its predecessor TM3, with improvements to the advection scheme, vertical diffusion parameterization, and meteorological preprocessing of the wind fields. Details of these improvements are described in separate papers and summarized in *Krol et al.* [2004].

[14] The so-called 'slopes' advection scheme of *Russel and Lerner* [1981] was extended to allow for two-way nested grids. *Berkvens et al.* [2000] and *Krol et al.* [2001] describe the details of this algorithm, which is both positive definite and mass-conserving. The algorithm allows several layers of nesting (such as Global 6×4, Northern Hemisphere 3×2 and Europe on 1×1) as well as multiple nested regions (such as Global 3×2, Asia 1×1, and Europe 1×1). In the two-way nested approach, information is communicated from coarser to finer resolutions, and vice versa. Thus, air masses originating from a nested region can leave that domain, circumvent the hemisphere (timescales of weeks), and impact sites in the nested grid again carrying more information than obtained with simple one-way nesting.

[15] The preprocessing of the offline ECMWF meteorological fields used in TM5 has been re-designed [*Segers et al.*, 2002] to perform all interpolation and re-gridding in the spectral domain. This creates greater consistency in mass-fluxes and more realistic wind fields, which can have a significant impact on transport of tracers [*Bregman et al.*, 2003]. In order to better capture the diurnal growth of the atmospheric boundary layer (BL), diffusion parameters (K_{zz} values) for the vertical diffusion scheme are now provided every 3-hours instead of every 6-hours. These are calculated offline at each TM5 resolution using the (spectral) mean winds and surface characteristics from ECMWF in the same way as is done in the parent model. In a newer version of

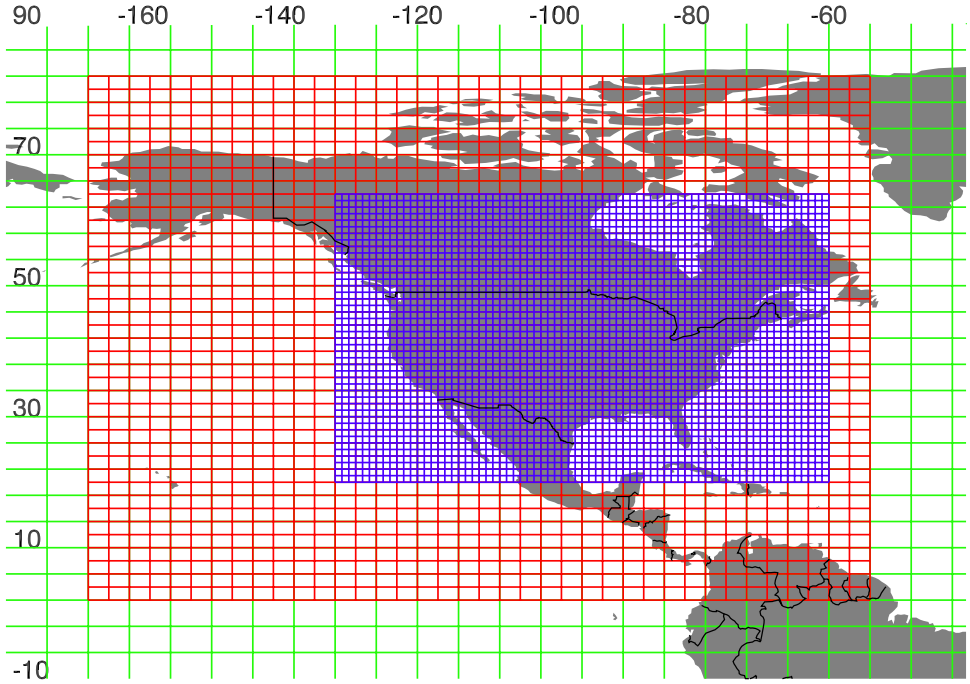

Figure 2. Map showing the different resolutions of TM5 used in this study. Note that the 6×4 grid extends over the global domain; the figure has been cropped to show more detail in the nested grid region.

TM5 these calculations are done online to save storage space. BL stability is calculated with the non-local closure scheme of *Holtslag and Boville* [1993] where previously *Louis* [1979] was used. The *Holtslag and Boville* [1993] scheme was adopted to stay consistent with the ECMWF parent model and to improve exchange between the BL and free troposphere. The need for improvements was first suggested by *Dentener et al.* [1999] from a comparison with and the implementation was tested by *Jeuken et al.* [2001]. Once the ERA-40 reanalysis (see http://www.ecmwf.int/research/era/) has been completed, TM5 will use 3-hourly convective mass-fluxes to replace the currently used online convection parameterization [*Tiedtke*, 1993]. The currently available set of preprocessed input data spans the period from January 1999 to November 2003.

2.3. Experiments

[16] TM5 runs were performed for January 2000 to November 2003 using three different model configurations: Global 6×4 (no nested regions), Global 6×4 with North America 3×2 (one nested region), and Global 6×4 with North America 3×2 with United States 1×1 (two overlapping nested regions). Figure 2 shows the model grid in these experiments. TM5 was initialized with a simple, self constructed SF_6 distribution that coarsely resembled the observed meridional and vertical gradients. Subsequently, the model was run to build up a self-consistent distribution of SF_6 during five years of spin-up, using the EDGAR-95 distribution [*Olivier and Berdowski*, 2001] of SF_6 emissions scaled to match the 1999 observed global total growth rate of SF_6 in the atmosphere.

[17] The results presented here were started from that point with 2000–2003 ECMWF meteorological fields, and the EDGAR-95 SF_6 emissions scaled to match the observed global atmospheric growth rate of SF_6 for those respective years (see Table 2). The global total emissions of SF_6 show a decline during 1999–2001 followed by a strong increase in 2002 that continues into 2003. This ~20% increase in emissions is derived from a similar increase in the atmospheric growth rate of SF_6 observed at remote background sites in the NOAA-CMDL network. The increase in growth rate is also seen at a subset of sites running quasi-continuous SF_6 analyzers. The cause of this increase in global SF_6 emissions is currently under investigation. Further discussion of SF_6 emissions will be in Section 10.

[18] The initialization procedure was chosen because the true atmospheric distribution of SF_6 at 1 January 2000 is not fully known and can thus not be prescribed to the model. Although an initial SF_6 field could be constructed from the observations, these would be too sparse to accurately prescribe concentrations in the upper troposphere. Mismatches between the assumed and true SF_6 distribution would lead to false gradients and trends in the model and complicate our analysis. Moreover, a prescribed SF_6 field is not necessarily consistent with the model calculated one, which emerges only after several years of spin-up. These problems are avoided in the approach we chose. The only consequence is that a global offset exists between the modeled and observed SF_6 abundance, representing the difference between the global total SF_6 amount TM5 was initialized with, and the true (but unknown) atmospheric amount of SF_6 on 1 January 2000. We account for this offset by adding a global constant amount of SF_6 to the model. This global value is calculated from the observed and modeled SF_6 distribution and takes into account the full seasonal cycle and latitudinal distribution (i.e., this offset is not biased towards the time or place where most measurements were available).

Table 1. Sites Used in This Study

Code	Lon, °	Lat, °	Alt, m	Name
		Surface Air Sampling Sites		
ALT	−62.52	82.45	210	Alert
ASC	−14.42	−7.92	54	Ascension
ASK	5.42	23.18	2728	Assekrem
AZR	−27.38	38.77	40	Azores
BAL	16.67	55.50	7	Baltic
BME	−64.65	32.37	30	Bermuda East
BMW	−64.88	32.27	30	Bermuda West
BRW	−156.60	71.32	11	Barrow
BSC	28.68	44.17	3	Black Sea Constanza
CBA	−162.72	55.20	25	Cold Bay Alaska
CGO	144.68	−40.68	94	Cape Grim
CHR	−157.17	1.70	3	Christmas Island
CRZ	51.85	−46.45	120	Crozet
EIC	−109.45	−27.15	50	Easter island
GMI	144.78	13.43	2	Guam
HBA	−26.50	−75.58	10	Halley Bay
HUN	16.65	46.95	344	Hungary
ICE	−20.15	63.25	100	Iceland
IZO	−16.48	28.30	2360	Tenerife
KEY	−80.20	25.67	3	Key Biscayne
KUM	−154.82	19.52	3	Cape Kumukahi
KZD	77.57	44.45	412	Kazakhstan, Sary Taukum
KZM	77.88	43.25	2519	Kazakhstan, Plateau Assy
LEF	−90.27	45.93	868	Park Falls
MHD	−9.90	53.33	25	Mace Head
MID	−177.37	28.22	4	Midway
MLO	−155.58	19.53	3397	Mauna Loa
NWR	−105.58	40.05	3475	Niwot Ridge
POC[a]	−163.00	35S–45N	10	Pacific Ocean Cruise
PSA	−64.00	−64.92	10	Palmer Station
PTA	−123.73	38.95	17	Point Arena
RPB	−59.43	13.17	45	Ragged Pt Barbados
SEY	55.17	−4.670	3	Seychelles
SHM	174.10	52.72	40	Shemya
SMO	−170.57	−14.25	42	Samoa
SPO	−24.80	−89.98	2810	South Pole
STM	2.00	66.00	7	Station "M"
SYO	39.58	−69.00	11	Syowa
TAP	126.13	36.73	20	Tae-ahn Peninsula
TDF	−68.48	−54.87	20	Tierra del Fuego
UTA	−113.72	39.90	1320	Utah
UUM	111.10	44.45	914	Ulaan Uul Mongolia
WIS	34.88	31.13	400	Negev Desert, Israel
WLG	100.90	36.29	3810	Mt Waliguan
ZEP	11.88	78.90	475	Zeppelin Mt, Svalbard
		Vertical Profiling Sites		
HFM	−72.17	42.54	500–7500	Harvard Forest
CAR	−104.80	40.90	3000–8000	Colorado (CARR)
PFA	−147.29	65.07	1500–7500	Poker Flats
HAA	−158.95	21.23	500–7500	Hawaii
RTA	−159.83	−21.25	500–4500	Rarotonga
		High Frequency Sites		
BRW	−156.60	71.32	11	Barrow
HFM	−72.17	42.54	340	Harvard Forest
NWR	−105.58	40.05	3018	Niwot Ridge
MLO	−155.58	19.53	3397	Mauna Loa
SMO	−170.57	−14.25	77	Samoa
SPO	−24.80	−89.98	2810	South Pole

[a]Flask samples filled during ocean cruises between 35°S and 45°N at 5° intervals.

The global offset amounted to 1.55 ppt by which the modeled fields were increased prior to the analysis.

2.4. Data Selection and Processing

[19] SF_6 observations from 68 sites operating during 2000–2003 were used in this study (Figure 1). In this figure, sites indicated by triangles are MBL sites, as they are far away from sources of SF_6. Observations at MBL sites were used with methods similar to *Masarie and Tans* [1995] to define the meridional gradient. Table 1 lists the three letter site codes used throughout this work for each location.

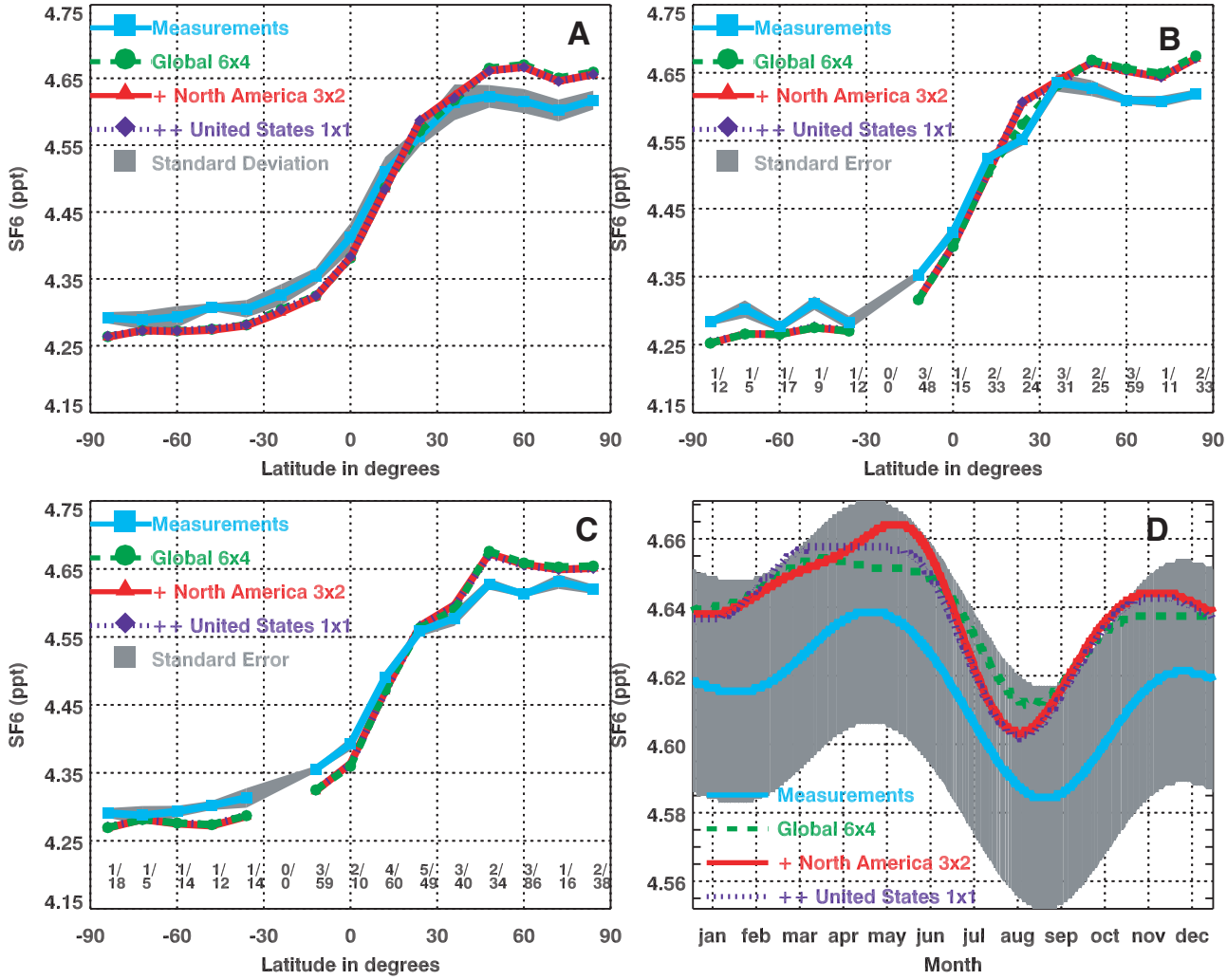

Figure 3. (a) Average annual meridional gradient of SF_6 for 2000–2003. The gray shaded area denotes the standard deviation of the 12-month average for each latitude (b) January meridional gradient, gray shaded area denotes the standard error resulting from averaging multiple sites and measurements in a given month and latitude bin (c) same as b, for July (d) Mean seasonal cycle of SF_6 for all MBL sites between 30°–60°N; gray area denotes the residual standard error resulting from fitting a seasonal curve to the full time series for all sites within the latitude bin. TM5 results in the same Figures are represented by three curves as indicated in the labels on the plots. Numbers on b and c denote the number of sites in a latitude band (top) and the number of samples in the mean (bottom).

[20] Modeled SF_6 mixing ratios were sampled at the same times flasks were filled for each of the sites and interpolated to the exact geographical location of the site using a 3D volume interpolation. Interpolated model results were compared to simple gridbox sampling; differences were generally small due to the long lifetime and small local gradients of SF_6. Data that were flagged were not used in this analysis. The data from aircraft measurements were binned to altitude for each flight, representing vertical levels at approximately 500m intervals. This ensures an objective comparison to modeled SF_6 values, which were sampled at the same discrete altitudes in the model. Seasonal cycles from the three year time series and their standard deviations were made with the curve fitting procedures described in *Thoning et al.* [1989]. Prior to our analysis, modeled and observed SF_6 time series were detrended using the observed 2000–2003 global trend of 0.210 ppt/yr.

3. Meridional Gradient

[21] Figure 3a shows annual mean SF_6 in 15 latitude bins constructed from measured and modeled surface concentrations at 40 MBL sites (see Figure 1). Clearly, TM5 overestimates the observed gradient, as was the case for the eleven models used in the TransCom experiment. The relative magnitude of the overestimate is similar as well (19% of the measured average gradient between the latitudes 90°S–30°S and 30°N–90°N), although the absolute gradients are smaller here because later years with lower emissions were used. Note that although the figure suggests most of this overestimate to be in the Northern Hemisphere,

the modeled concentrations were scaled to the observed global mean value of 4.44 ppt and might thus not accurately reflect the location of these over and underestimates. Previous results from TransCom suggest however that Southern Hemisphere sites are reproduced quite well by these types of transport models, and that the overestimate is mostly in the Northern Hemisphere.

[22] The observed meridional gradient shown here incorporates many more observations than those used in previous studies, which allows us to calculate the gradient for individual months, and construct seasonal cycles. Figures 3b and 3c contrast the January gradient with the one in July. Figure 3d shows that despite emissions that are constant in time, surface SF_6 abundances at NH mid-latitude MBL locations decrease in summer. This is due to greater vertical mixing over the continents in summer than in other seasons, transporting SF_6 to the free troposphere instead of trapping it in the PBL and advecting it towards the oceans. Figure 3d shows that the timing of this seasonal change is well captured by TM5 at typical NH mid-latitudes. The amplitude of this relatively weak seasonal signal (0.06 ppt peak-to-trough) is somewhat smaller than in the observations, but still within the large standard deviation.

[23] The interhemispheric exchange time calculated for TM5 from the modeled 3D SF_6 distribution is 0.90 years in a non-steady state approach (i.e., $\tau = 2\Delta M/(\Delta E - d\Delta M/dt)$ with M = SF_6 mass, E = Emissions, and Δ refers to the difference NH-SH, the $\Delta M/\Delta t$ term is a correction for the yearly growth of the gradient, formulation is analogous to *Denning et al.* [1999]). When just using surface SF_6 values (2D), the exchange time is 1.5 years. Compared to the TransCom models mentioned earlier, TM5 is average in the 2D exchange time, and on the slow side for the 3D values. Both exchange times are faster than the version of the TM3 model used in TransCom though. Budget analysis shows that SF_6 reaches the SH mostly in the free troposphere as a small 'leakage' from the SF_6-rich Hadley cell circulation in the NH. This leakage is less than $\sim$5% of the SF_6 transported into the tropics from the NH, but nevertheless accounts for 95% of the input of SF_6 to the SH due to the sparse emissions there. An experiment with doubled strength of convection decreased the overestimate of the meridional gradient to $\sim$17% due to larger fluxes in the Hadley circulation and more leakage, but it is by far not enough to explain the observed differences. Other factors influencing the meridional gradient include the latitudinal distribution of SF_6 emissions and the efficiency of stratosphere-troposphere exchange, which we will discuss in Section 10.

[24] There is very little variation among the different TM5 configurations, with the nested versions showing a slightly smaller meridional gradient and a slightly larger winter-summer amplitude at the NH than the Glb 6×4 simulation. These differences are generally smaller than the differences observed among different models. For instance the overestimate of the meridional gradient between SPO ($-90°$S) and BRW (71.3°N) is 19% for the three simulations in this study, but shows a much wider range for similar transport models participating in an ongoing transport model intercomparison (EverGreen, P. Bergamaschi, personal communication, 2004). Even with models that use the same ECMWF wind fields and the same parameterizations for vertical mixing, the differences are larger than that from our nested grid approach. This indicates that the nested grid has a very minor influence on the global SF_6 distribution as observed at remote locations. It supports TM5's nested grid approach, since it shows that the model can be used to resolve a region of interest to a high degree without changing the simulation of global scale features. It also supports the suggestion in *Denning et al.* [1999] that there is no relation between horizontal model resolution and the success in representing the meridional gradient of SF_6.

4. Land-Sea Gradients

[25] A second important gradient to analyze is that between MBL and continental sites. With new sites being added predominantly on continents, this is an important new source of information for transport evaluation. To visualize this gradient for SF_6, we have taken the monthly mean SF_6 value for each non-MBL site and subtracted the average MBL value at the corresponding month and latitude (as shown in Figures 3b and 3c). The resulting value will from here on be referred to as the "land-sea gradient" for a particular site.

[26] Figure 4a shows the modeled vs observed annual mean land-sea gradients. The 0.08 ppt level indicated by a gray shaded area centered around the 1:1 line is twice the standard deviation of similarly calculated gradients displayed by MBL sites. Gradients exceeding this value are thus significantly larger than those encountered for a set of MBL sites only. Most non-MBL sites appear to fall within this range, indicating that they are not all that different from MBL locations. The cloud of points between -0.08 and 0.03 ppt, however, represents mostly remote non-mbl sites such as TDF, sites on mountain tops such as WLG, ASK, IZN and NWR, and aircraft measurements such as from CAR, PFA, and HAA which are not included as MBL sites. The real "continental" locations are indicated in the figure by their three letter site codes. These sites show an observed land-sea gradient on the order of $\sim 0.0-0.2$ ppt, whereas the model calculations systematically display stronger gradients. Although some of these overestimates disappear when increasing the resolution (e.g., PTA), others benefit very little from this (e.g., UTA) or result in larger gradients (e.g., HFM, KEY). The observed seasonal change of the land-sea gradients (not shown) is generally quite small (<0.1 ppt), and systematic differences between modeled and measured land-sea gradients as a function of season could not be detected. The largest changes in observed land-sea gradients occur mostly at sites in the free troposphere (CAR, HAA, HFM, PFA) and high altitude sites (WLG, KZM, ASK). These sites display less synoptic variability, less influence from local sources, and therefore more clearly show the effect of seasonal SF_6 enhancements through increased vertical exchange. The fact that such signals are more easily detectable in the free troposphere stresses the importance of vertical profile measurements of SF_6. Further examination of continental sites will be presented in Section 8.

5. Vertical Gradients

[27] A set of regular vertical profiles through the lower 8 km of the troposphere is now available for a number of

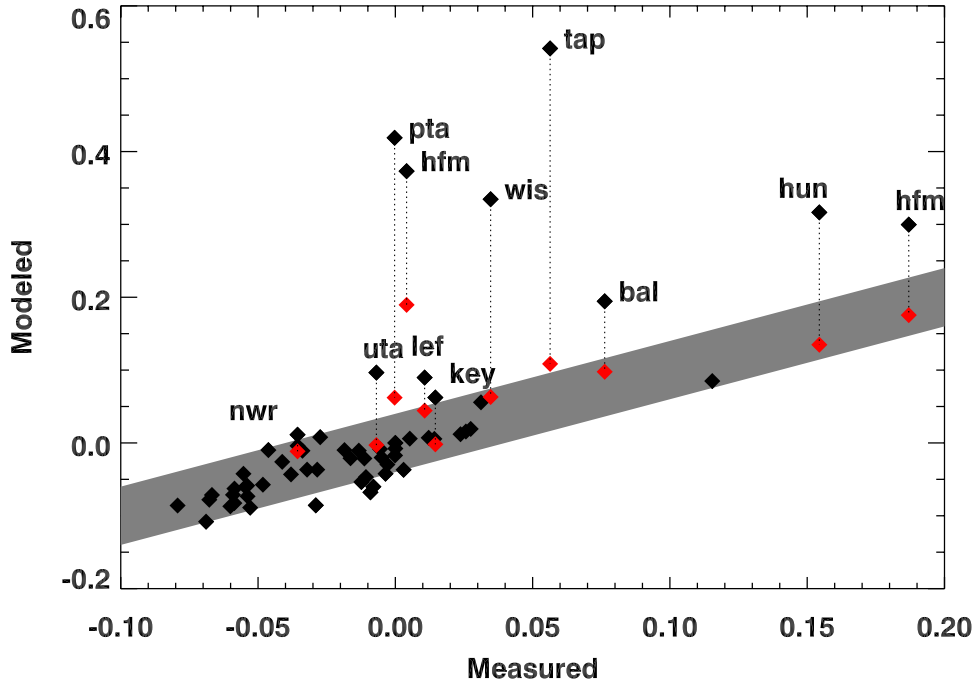

Figure 4. Measured and modeled annual mean land-sea gradient (see text) for non-mbl sites; large discrepancies are indicated by their three letter site codes. Gray shaded area indicates 0.04 ppt difference between measurements (x-axis) and model (y-axis). Results displayed are for a run with one nested region, Global 6×4 and North America 1×1 are similar to the ones shown. Red diamonds are model results for a run with more vigorous vertical mixing, discussed in Section 6.

locations listed in Table 1. There are enough data to construct binned altitude profiles for 3-monthly intervals describing the seasonality of the vertical gradient at each site. Figure 5 shows these for each location, together with modeled profiles that are co-located in time and space with the original aircraft samples.

[28] The first feature that stands out is the small magnitude of the vertical SF_6 gradient at most sites. With the exception of HFM, gradients do not exceed 0.2 ppt. Partly, this reflects the still sparse record, as the 1-σ standard deviations indicate that the variability around the mean is quite significant. Furthermore, the observations were mostly made at remote locations where SF_6 was well-mixed throughout the troposphere. The only SH site, RTA, shows a reversed gradient of SF_6 because the free troposphere is supplied with SF_6-rich air through inter-hemispheric transport, whereas the MBL is more distant from SF_6 sources. At HFM, the frequency with which SF_6 rich air from the direction of New York city (∼250 km away) reaches the site increases by ∼25% in summer (analyzed from wind-sector data reported for this site). The seasonal change of surface SF_6 at HFM was found to reflect these events more strongly than the effect of vertical exchange, and might therefore be less useful in this analysis. Several other important features can be seen in the figure.

[29] 1. Although surface SF_6 is significantly overestimated at HFM, CAR, and PFA, this does not seem to result in an underestimate of SF_6 in the free troposphere elsewhere in the NH. The seasonal transport patterns seen at upper tropospheric sites show that the NH free troposphere is quite sensitive to the supply of SF_6 from below. The fact that we don't see large discrepancies in the free troposphere suggests that the surface overestimate is a local feature and SF_6 does escape the BL eventually. We will investigate this further in Section 6.

[30] 2. Despite the good agreement at NH free tropospheric sites, RTA does not receive enough SF_6 in the model at any altitude. The offset is ∼0.04 ppt for all seasons and all altitudes. This is one of the largest discrepancies seen in Figure 5, and is very similar to the overestimate of the meridional gradient. Both the offset at RTA, and the overestimate of the meridional gradient are caused by either a lack of inter-hemispheric exchange in TM5, or a lack of emissions in the SH in our inventory. We will discuss this further in section 10.

[31] 3. All sites display an increase in free tropospheric SF_6 from December-January-February (DJF) to June-July-August (JJA), decreasing the vertical gradient (with the exception of RTA, where an increase in free tropospheric SF_6 causes an increase in the JJA vertical gradient). This

Figure 5. Vertical profiles of SF_6 for four seasons from five sites: CAR, HFM, HAA, RTA, PFA. Observations and model were binned to specific altitudes. SF_6 values are on the x-axis, the number of profiles averaged in each season is displayed on the righthand side of each figure. Gray shades on the observations (blue line) denote the standard error of the mean; the grey bars denote the standard deviation of the mean. TM5 results from the single-nested run are included as a red line; other resolutions show similar results. All sites except HFM are shown on a 0.25 ppt range.

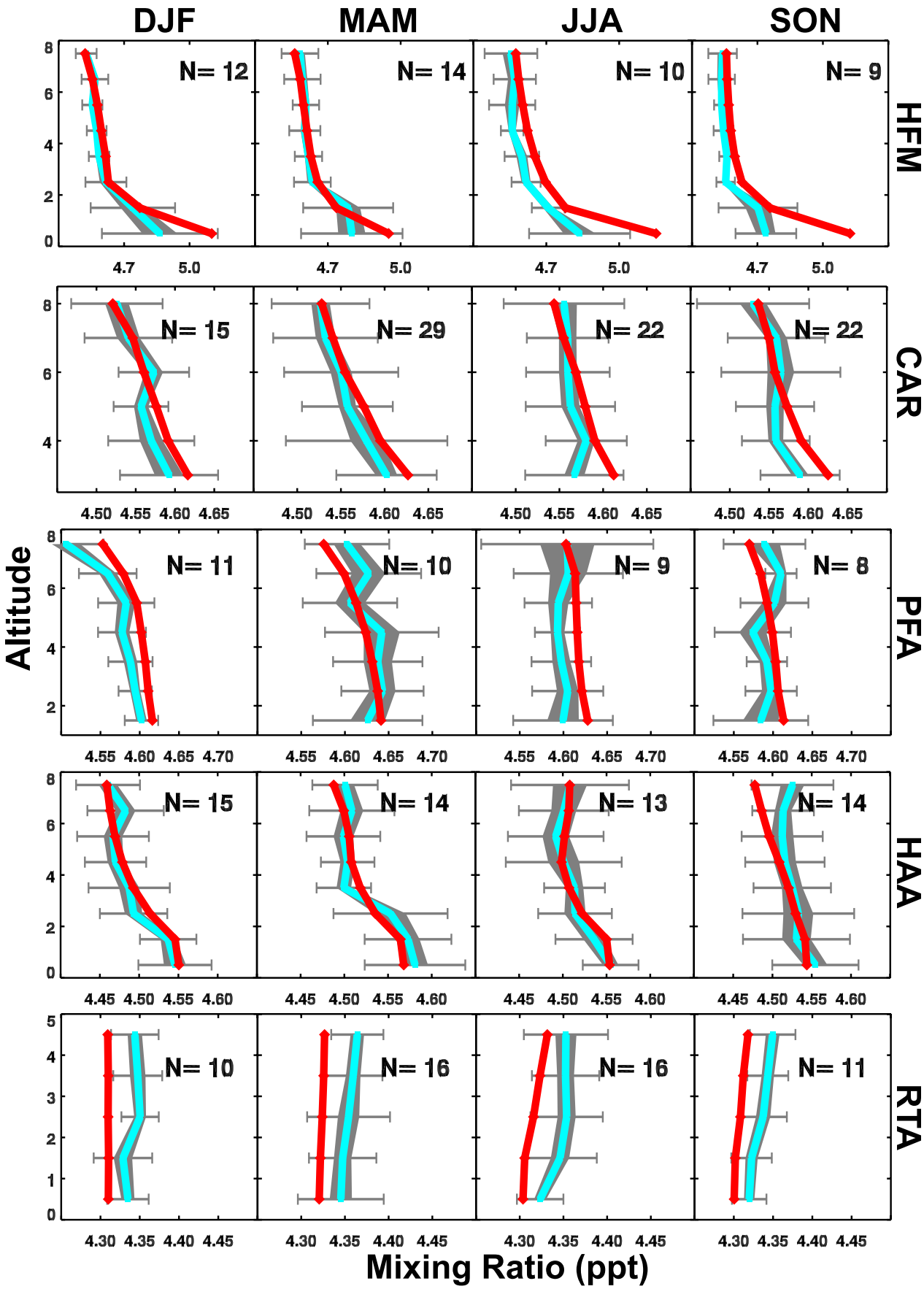
DJF
MAM
JJA
SON
HFM
CAR
PFA
HAA
RTA
N= 12
N= 14
N= 10
N= 9
N= 15
N= 29
N= 22
N= 22
N= 11
N= 10
N= 9
N= 8
N= 15
N= 14
N= 13
N= 14
N= 10
N= 16
N= 16
N= 11
Altitude
Mixing Ratio (ppt)

Figure 5

change in vertical gradient is directly related to the strength of vertical mixing in summer and links the observed changes in the meridional and land-sea gradients to vertical transport. TM5 reproduces these increases reasonably well; the model-measurement differences at the highest level in JJA are not significant except at RTA. This suggests that TM5's vertical exchange is fairly good and does not have large biases in time or magnitude.

[32] The main difficulties in interpreting the comparison of vertical profiles is that the number of locations is small, the vertical gradients are weak, and the observed differences are only just statistically significant. The latter is due to the large variability relative to the observed gradient and the still limited number of measurements in each season. Comparison to individual profiles shows that TM5 reproduces the variable shape and magnitude of the vertical gradients very well. These are not shown here though, since the standard deviation on individual profiles often exceeds the gradient itself making any differences not relevant in a statistical sense. A significant improvement in measurement precision would be very useful to diagnose the small seasonal changes and vertical gradients with more confidence. Also, ongoing extension of the network of vertical profiling stations can perhaps help draw a clearer picture in the near future.

6. Boundary Layer Mixing

[33] TM5's inability to reproduce land-sea gradients and surface SF_6 mixing ratios for continental sites is directly related to vertical mixing in the PBL. The good agreement at MBL and free tropospheric sites suggests that SF_6 is mixed through the vertical column sufficiently between the time of emissions and detection for remote sites, but not for sites closer to the sources. Faster mixing of surface emissions through the PBL could possibly remedy this. An experiment using the original vertical diffusion parameterization, but doubled diffusivity coefficients showed only little response because the dynamic range of K_{zz} values is very large. Linear, global scaling factors are thus not very helpful in increasing mixing. Therefore, the diffusion scheme was replaced by a simple algorithm that completely mixed all SF_6 from the surface up to the boundary layer height diagnosed by the ECMWF parent model. K_{zz} was taken as 1.e3 m^2s^{-1}, which corresponds to a mixing time of 17 minutes for a 1000 m deep BL, and 67 minutes for a 2000 m deep BL ($\tau = BLH^2/K_{zz}$). Figure 4 shows the comparison to observations in red diamonds. The enhanced mixing brings all continental sites in much closer agreement, mostly within the 0.04 ppt bounds. The other non-MBL sites in the free troposphere are hardly affected, and concentrations at MBL sites (not shown) do not change appreciably. The meridional gradient is not affected by enhanced PBL mixing (1% decrease in gradient), and vertical profiles above the PBL show little to no response to this measure. This partly confirms the earlier statement that this reservoir is too large to accurately diagnose small changes in mixing. Other improvements (not shown) include a better representation of seasonal cycles at HUN, UTA, and BAL.

[34] This sensitivity of modeled SF_6 to the efficiency of PBL mixing is an important result, especially since faster mixing influences annual mean CO_2 concentrations considerably (see Section 9). Many other models participating in TransCom suffered from a similar overestimate of SF_6 at continental sites, and we speculate here that similar shortcomings in PBL mixing efficiency are responsible. An important next step is to find out when (night/day, summer/winter) and where (PBL/MBL, tropics, mid-latitudes) the current mixing scheme fails. For instance, the need for more efficient mixing in the PBL might be limited to certain stability regimes and thus depend on the Richardson number, or it could be required only at a certain distance to sources to compensate for representation errors in the model. Although SF_6 is shown here to help in such diagnosis, it also requires higher frequency data, vertical profiles in the BL, and shorter lived compounds (see Section 10). A detailed study of PBL mixing in this type of model should have high priority, but is beyond the scope of this work. Finally, we stress that although the current simplification of the mixing scheme works well for SF_6, this might not be the case for CO_2 or other compounds with different emission distributions and should therefore not be seen as a final solution to the problem of too slow mixing of the PBL in TM5.

7. Temporal Variability

[35] On seasonal time-scales, TM5 performs well on all three resolutions. Figure 6 shows the measured and modeled seasonal cycles of SF_6 at MID, BRW and LEF. We chose these sites as they represent different regions, latitudes, and signals close to, or in, our two-way nested domain. Generally, the seasonal cycle of SF_6 is small compared to variability on higher frequencies, reflecting the lack of seasonal variations in emissions. The standard deviation of the seasonal cycle is therefore relatively large (grey bar), especially at LEF which is close to SF_6 sources. Note that between 10–20 individual measurements were used to construct these seasonal cycles and that the standard error on these curves is much smaller than the standard deviation.

[36] The seasonal cycles at MID, and BRW reflect the enhanced continental mixing in NH summer, causing less SF_6 to be transported horizontally. TM5 nicely reproduces the timing of the seasonal cycle, as well as the amplitude. At the continental tower site LEF, the seasonal cycle has two maxima; one in spring and a smaller one in early winter, with the typical NH summer minimum in between. Although build-up of SF_6 early in the year, and a minimum in summer are reproduced by the model, the overall fit is neither impressive nor significantly wrong most of the time. The complicated behavior at LEF is partly due to the close proximity of SF_6 sources. The seasonal cycles at tropical sites such as SEY, GMI, ASC, and SMO (not shown) indicate that the passage of the ITCZ is timed well in TM5, and it causes increases/decreases in modeled SF_6 very similar to those observed. Only at SMO, which is quite far south in the SH tropics (14°S), an SF_6 underestimate is seen in January and February when NH air reaches this location regularly [*Prinn et al.*, 1983; *Peters et al.*, 2001]. This suggests that NH air does not penetrate deeply enough into the SH and could contribute to the overestimated north-south gradient in TM5.

[37] Figure 7 shows observations at several locations where high frequency in situ SF_6 measurements are made

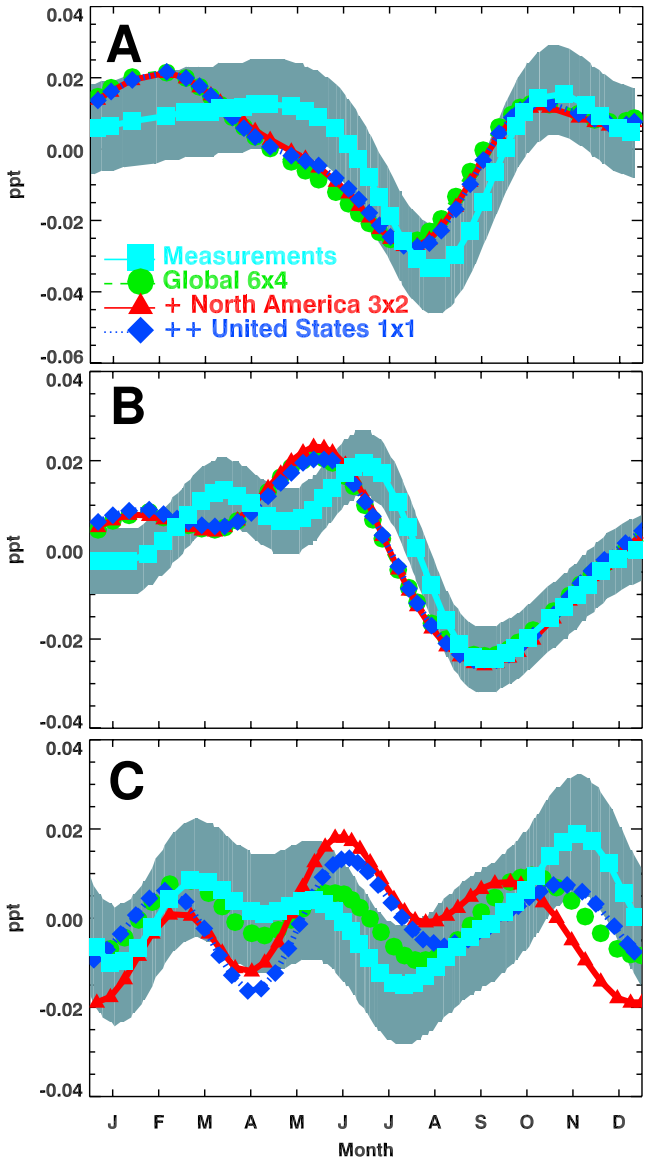

Figure 6. The detrended seasonal cycle of SF_6 at (a) MID (b) BRW and (c) LEF for different model resolutions. The means of the seasonal cycles were normalized to zero. Gray shading indicates the residual standard error resulting from fitting a seasonal curve to the full time series. Modeled SF_6 curves are plotted on top and colored according to the label in the Midway plot.

by the NOAA CMDL Halocompounds and other Atmospheric Trace Species (HATS) group. The months shown in Figure 7 were chosen to represent both winter and summer months at MBL and continental sites, and our aim is to illustrate typical behavior at these locations.

[38] Observed temporal variability at sub-weekly scales is reproduced well by TM5. Synoptic variability changes flow regimes on scales of 2–5 days, such as seen at NWR in February 2002 (Figure 7a). TM5 reproduces SF_6 changes as large as 0.15 ppt. Again, HFM (Figure 7b) shows periods with relatively good agreement that are interspersed with periods of large model overestimates, corresponding to southwesterly winds from the city of New York. Enhanced mixing in the PBL (not shown) cannot bring full agreement between model and observations here. Interestingly, the finest resolution shows the highest overestimate despite the fact that it is separated from the city by the largest number of gridcells. The initial concentration after emission is much higher though, and our mixing scheme cannot disperse SF_6 quickly enough during transport. Finally, Figure 7c shows the time-series at MLO, where the variability is much smaller. Nevertheless, TM5 captures the transport regime change on day 14 adequately. The different resolutions of the model show the largest differences over HFM whereas the other sites are not sensitive to the grid size.

8. Continental Sites

[39] Considering the results from the previous sections, it is clear that horizontal nesting mostly affects continental sites and short (<month) time-scales. Differences between the three TM5 results are partly due to better resolved atmospheric transport, and partly due to better resolved spatial fluxes. An example of this is seen in Figure 8a, where the modeled monthly time series at PTA is shown, along with a map of the area. The positions of the 6×4, 3×2, and 1×1 grid boxes are plotted as well. There is a large representation error at 6×4, where emissions from nearby Sacramento are added directly to the grid box the site is located in. As a result, modeled SF_6 is strongly overestimated. This representation error disappears when a 3×2 degree nested region is included, making the site much more representative of clean, oceanic conditions. Adding a 1×1 degree region does not improve the simulation further.

[40] The opposite situation occurs at another coastal location, KEY. In Figure 8b, the 6×4 degree simulation most accurately follows the measurements. This is due to SF_6 from Miami, emitted into grid boxes that have an increasingly less oceanic, and more continental character going to smaller resolutions. To separate the city from the site, model resolutions of less than 20 km should be employed. In the past, situations such as these were resolved by moving the site in the model one or two grid boxes into the ocean thus assuring clean air to be sampled in accordance with the sites sampling strategy. This is still an option, with the added advantage that 1–2 grid boxes represent only 100–200 km in the finest nested domain instead of 400–600 km on the global domain. This ensures that the meteorology at the "virtual" site in the model much more closely resembles the actual meteorology at the site, minimizing the potential for errors and biases. An example of this using ^{222}Rn in TM5 is shown in *Krol et al.* [2004].

[41] Situations similar to these examples are much more likely to occur with continental sites, since they are located closer to point sources of SF_6. This poses stricter demands on the model performance and on the selection of data, and the weight one can assign to these locations in an inversion. We suggest that for every continental site used in an inversion, a brief study should be performed to assess local meteorology, the heterogeneity of the surrounding area, and the potential for representation error. We note that the unique nesting capabilities of TM5 warrant extra caution, because representation errors vary with the grid-size which can vary for different simulations.

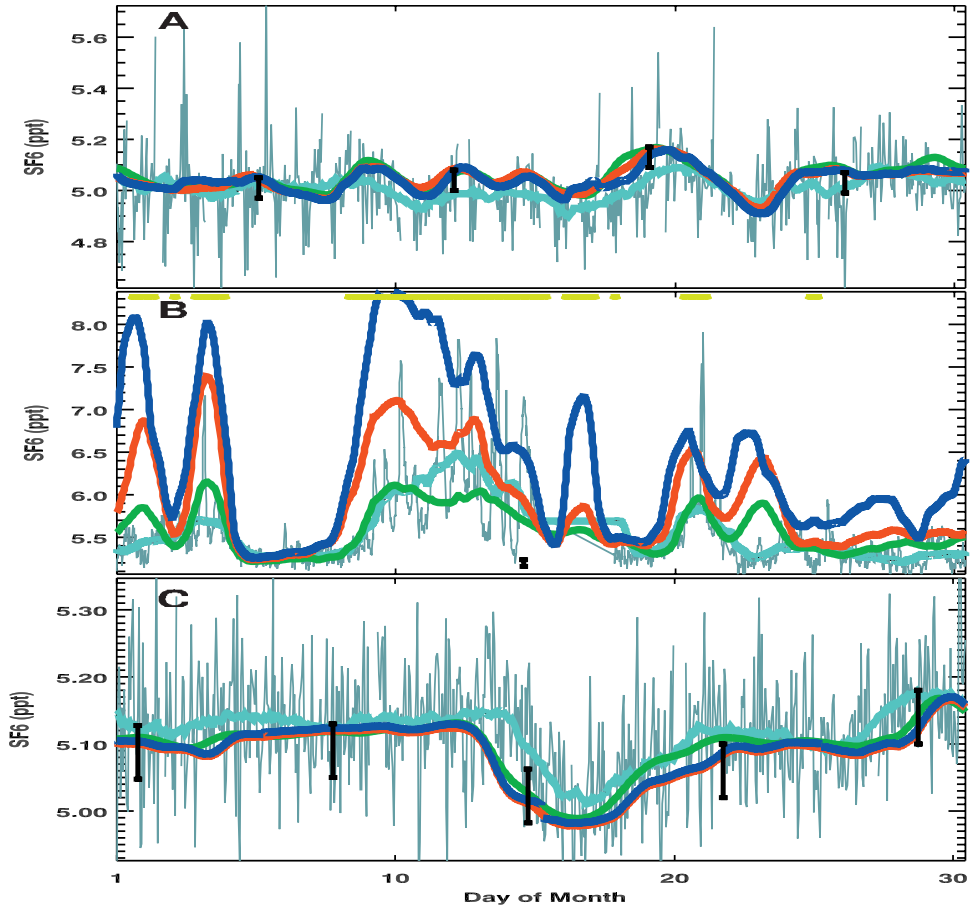

Figure 7. Hourly time-series of SF_6 at sites (a) NWR, Feb 2002 (b) HFM, Aug 2002 and (c) MLO, Oct 2002, compared to TM5 with different nested resolutions: Global 6×4 (green), +North America 3×2 (red), ++United States 1×1 (blue). All curves were smoothed with a 24-hour boxcar average; original (unsmoothed) measurements shown in grey with a lightblue 24-hour average. Flask measurements are shown as black bars with 0.04 ppt measurement uncertainty around the central value. The yellow horizontal lines on top of the HFM plot show periods with southwesterly winds, bringing air from New York. Note that the unsmoothed measurements (grey) represent mostly instrument noise, and not real hourly variability.

[42] Overall, the differences between the three resolutions are quite small, and do not reveal a distinct advantage of the nested grids. This is mostly due to our choice of SF_6 as transport tracer, which has a very long life-time and can be considered well mixed in the atmosphere. The largest gradients are the meridional gradient, followed by land-sea gradients and temporal gradients due to synoptic events. These three gradients can be quite well represented on a coarser grid. Also, the emissions of SF_6 relative to the location of the majority of our sites effectively make them 'point sources', with large areas showing near-zero emissions. For tracers that have stronger gradients in their source distribution (e.g., CO_2), or larger atmospheric gradients due to chemistry (e.g., NO_x, O_3, SO_2, ^{222}Rn) or meteorology (e.g., arctic vortex), zooming leads to more obvious improvements [*Krol et al.*, 2004; *van den Broek et al.*, 2003].

9. Implications for CO_2

[43] An important goal of NOAA CMDL is to achieve an improved understanding of the carbon cycle. One way in which SF_6 is connected to the carbon cycle is through a concept called the 'seasonal rectifier' [see also *Denning et al.*, 1995; *Law*, 1996; *Dargaville et al.*, 2000; *Chen et al.*, 2004]. The rectifier describes the covariance between seasonally changing emissions, and seasonally changing transport. For example, rectification can cause annual mean CO_2 surface concentrations to be non-zero even if the uptake balances the emissions over a year everywhere. Such a situation exists at locations where CO_2 fluxes from the biosphere are dominant. The uptake (photosynthesis) draws from a relatively large volume of air when the BL is deep in summer, whereas the emissions (respiration) affect a relatively small volume when the BL is more shallow in winter. Thus, concentrations at the surface are more strongly enhanced in winter than decreased in summer, and the annual mean is likely positive; a positive rectifier. Seasonal rectification is very strongly tied to vertical transport as this is a main driver of seasonal transport variations at mid-latitudes.

[44] If a model used for CO_2 inversions does not adequately capture such co-variations, biases in flux estimates

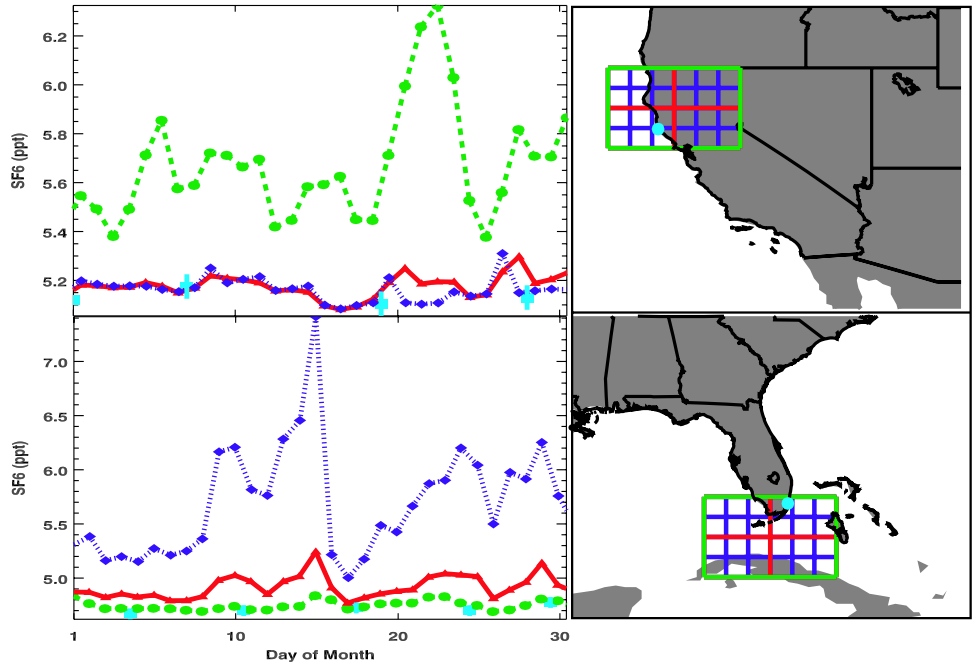

Figure 8. Modeled timeseries of SF_6 at two continental sites in the US: PTA, July 2002 (top), and KEY, May 2000 (bottom). The location of these sites is given in the right hand panel by light blue dots. Green boxes show the TM5 grid at 6×4 degree, red the 3×2, and blue the 1×1 degree resolution. Modeled SF_6 is plotted in the same colors as the corresponding grid. Measured SF_6 values are indicated by blue bars.

will be introduced as compensation for model errors. For example, a too shallow BL in winter will lead to overestimates in model predicted CO_2 at a nearby site, which can be compensated in an inversion by (incorrectly!) decreasing emissions in winter, or increasing uptake in the following summer. As the co-variance between transport and CO_2 surface fluxes is much stronger in the NH than in the SH, transport errors could also lead to false meridional gradients leading to trade-offs between tropical and extratropical fluxes, as seen in *Gurney et al.* [2003]. The ability to assess vertical transport with SF_6, which does not have seasonally varying emissions and has a relatively well-known source distribution is therefore of great value for CO_2 inversion studies.

[45] Figure 9 shows the annual mean CO_2 concentrations in TM5 for a 6×4° run with (a) slow PBL mixing, and (b) fast PBL mixing. These patterns were made by introducing seasonally changing CO_2 fluxes from the land biosphere (from the Carnegie Ames Stanford Approach model [*Randerson et al.*, 1997]) in the model. These fluxes balanced to a zero annual mean in each gridbox, and would thus give zero-concentrations in the absence of transport. The interaction with seasonally changing transport have led to non-zero annual means as described above. Such rectification patterns were also made for the eleven TransCom models to compare their seasonal transport characteristics [*Gurney et al.*, 2003].

[46] The difference in rectification between the two mixing schemes is quite large, up to 2.5 ppm in the annual mean. The better agreement with SF_6 at continental surface sites in the fast mixing case (see Figure 4, red diamonds) suggests that the smaller rectification pattern is more realistic. The less realistic slow mixing case would have compensated the positive annual mean concentrations by decreased respiration in winter, and increased photosynthesis in summer leading to an annual mean CO_2 flux estimate that was biased low in NH mid-latitudes. The eleven transport models in TransCom varied significantly in their degree of seasonal rectification [*Law*, 1996], and in their ability to simulate the observed SF_6 meridional gradient [*Denning et al.*, 1999]. It is likely that TransCom models in Family I (trapping over the continents, N-S gradient overestimated) all simulate too strong seasonal rectification and suffer from the same low-bias in CO_2 flux estimates in NH mid-latitudes. Our results also suggests that models with weaker seasonal CO_2 rectification will likely reproduce SF_6 observations better, and thus produce more robust CO_2 flux estimates.

[47] The source distribution of SF_6 strongly resembles that of fossil fuel CO_2, suggesting that in addition to biases introduced by seasonal rectification, a north-south bias in this aspect of the modeled CO_2 distribution will exist. Such a bias has important implications for the distribution of land and ocean sinks of CO_2 calculated through an inversion, as a 20% overestimate of the gradient of ~5 ppm [*Gurney et al.*, 2003] would amount to a ~1 ppm north-south CO_2 bias. Although this signal is smaller than that from seasonal rectification, this would again cause the model to increase land uptake in NH summer, or decrease in respiration in NH winter. However, *Gurney et al.* [2003] did not find a significant correlation between the estimated NH mid-latitude land sink and the fossil fuel gradient, whereas the strength of the seasonal rectifier did correlate with that sink. This suggests that errors in the seasonal rectifier, rather than those in fossil fuel gradients, will dominate flux estimate biases. Strong correlation between the NH mid-latitude land regions and the tropical land regions [*Gurney et al.*, 2003]

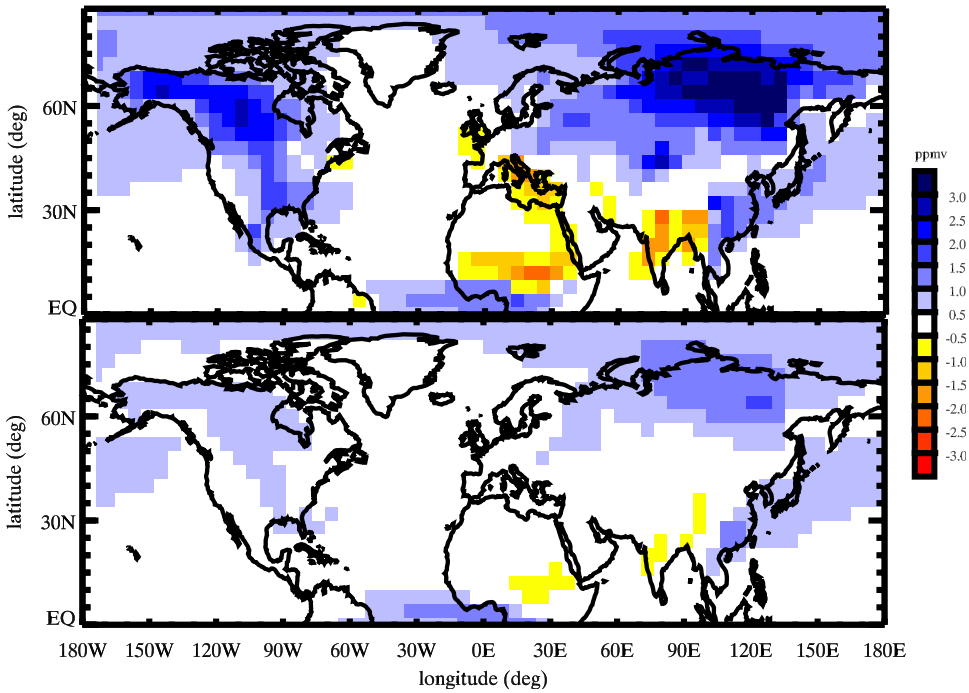

Figure 9. Annual mean concentrations of CO_2 from a 'neutral biosphere' experiment (yearly net-zero CO_2 fluxes in each land gridbox) with TM5 for (top) 'slow' vertical mixing and (bottom) 'fast' vertical mixing scenarios. Differences of up to 2 ppm between the two will lead to strongly different CO_2 fluxes in an inversion with each scenario, stressing the importance of correctly describing transport. See Section 9 for more information.

further suggests that overestimates in the land sink will be compensated by the poorly constrained tropical fluxes to maintain global mass balance. Further investigation of this bias and its effect on CO_2 flux estimates is part of ongoing research.

[48] The role of land-sea gradients in CO_2 in inversions is hard to estimate since few inversions were published that actually used data from continental sites. On the one hand, CO_2 temporal signals over the continents are large and could easily dominate the smaller land-sea (and even meridional gradients). *Law et al.* [2003] have shown that biases between sites of up to 0.2 ppm will hardly affect inversion results if continental sites with approximately weekly observations are introduced to the inversion. On the other hand, these gradients are driven mainly by vertical transport in the PBL over the continents, which needs to be modeled correctly to reproduce the strong diurnal and synoptic variability in CO_2. A strategy to assess and improve model transport on these smaller scales with in-situ observations currently does not exist for North America (it does exist in Europe through the AEROCARB www.aerocarb.cnrs-gif.fr and EverGreen http://www.knmi.nl/evergreen/projects), but it will be of great importance to gain confidence in the detailed flux estimates pursued by the NACP program.

10. Discussion

[49] The main difference between this work and the similar TransCom study of *Denning et al.* [1999] is the introduction of the TM5 transport model, which has the ability to refine the horizontal grid. Also, the measurements, model transport, sampling strategy, and emissions strengths are all consistent with each other in this work, whereas the TransCom study interpolated data and model calculations in time to increase the scope of the study. Finally, the availability of many new SF_6 measurements allows us to study the modeled and measured SF_6 distribution in space and time.

[50] Our analysis revealed two significant biases in modeled transport. First, the vertical mixing scheme used in TM5 does not distribute surface emissions through the PBL fast enough. This shows up as overestimates of SF_6 mixing ratios at continental sites and leads to a large overestimate of land-sea gradients in the model. Substituting the vertical mixing scheme in the model by a simple scheme that rapidly mixes the PBL up to its diagnosed altitude strongly improved the comparison to SF_6 observations at continental sites without adversely affecting remote locations or vertical gradients. Linear scaling of vertical diffusion intensity by up to factor of two did not achieve similar results due to the large range over which these values can vary. Recent work comparing diffusion coefficients from the ERA40 reanalysis with those generated for the TM3 model (and also used by TM5) did not reveal large differences (Olivié et al., "Evaluation of the vertical diffusion coefficients from ERA-40 with simulations", ACPD, submitted manuscript, 2004), and both methods showed similar success in reproducing observations of ^{222}Rn and BL heights. This suggests that problems with vertical tracer transport in TM5 are shared by the ECMWF parent model. Problems with too slow mixing of moisture were reported for the ECMWF model on high resolution (Jordi Vila, personal communication, 2004). Improvements in BL transport, including entrainment/detrainment formulations, day/night effects, and stable/

Table 2. SF_6 Emissions Estimates Based on the Observed Atmospheric Growth Rate (Used in This Study), and Emissions Estimated From the EDGAR Emission Database[a]

Year	Atmosphere[b]	Edgar	Edgar/Atm
1999	5060	5140	1.015
2000	5023	4550	0.906
2001	4957	4700	0.948
2002	5517	n/a	/
2003	5808	n/a	/
	Regional Emissions[c]		
USA		36.3%	
Europe		17.0%	
Japan		12.7%	
East Asia		10.1%	
Former USSR		5.9%	
Canada		4.3%	
Middle East		3.9%	
South Asia		3.6%	
South East Asia		2.0%	
Others		4.2%	

[a]Emissions are in 10^3 kg SF_6/yr. EDGAR yearly estimates provided by J. Olivier (personal communication, 2003).

[b]Emissions estimated from the observed atmospheric growth rate at MBL sites.

[c]Based on the EDGAR-95 spatial distribution; see http://arch.rivm.nl/env/int/coredata/edgar/.

neutral/convective formulations should therefore be developed based on new insights in PBL turbulence, as well as new atmospheric data to test new formulations in models such as TM5. The current 'fix' should be considered a simple sensitivity test in this respect, and not a solution to the problem of too slow mixing. In this respect, we also have to mention a possible role for horizontal diffusion. This process is usually not included in global models because numerical diffusion is believed to be large enough to ensure proper dilution. However, this process will become more important as models like TM5 use finer grids, and is already used in many regional scale models. The largest drawback here is that horizontal diffusion coefficients are usually poorly known, allowing horizontal diffusion to compensate for other transport problems in the model which is clearly unwanted.

[51] More insight into mixing on shorter time and spatial scales could be gained through continuous measurements. Such measurements will better reflect diurnal cycles and changes of stability regimes. Measurements of CO_2 at tall towers from NOAA CMDL could be useful in this respect, provided that the surrounding source and sink distribution is known adequately. Another viable candidate would be ^{222}Rn. This tracer has a much shorter lifetime than SF_6, displays much larger gradients in space and time, and it has more heterogeneous sources. It more strongly depicts synoptic meteorology including the effect of meso-scale convection and boundary layer growth. The latter is directly related to the seasonal rectifier and as such is important to study. Especially for continental locations (close to the sources), ^{222}Rn could bring more insight. ^{222}Rn measurements from European platforms are already used for transport model evaluation (such as EverGreen and AEROCARB). NOAA CMDL also plans to equip tall towers with ^{222}Rn measurement systems in the near future, presenting additional ways to study transport specifically in the US.

[52] The second bias is an overestimate of the meridional gradient by ~19% compared to observations. This bias exists irrespective of the use of a slow or fast PBL mixing scheme is, and it is not accompanied by a significant bias in land-sea gradients, or vertical gradients. A similar overestimate was seen for many models in the *Denning et al.* [1999] SF_6 study, and there it was suggested that these models had insufficient transport to the free troposphere, causing surface SF_6 to be overestimated, most strongly in the NH. However, the considerable number of vertical profiles presented here do not corroborate insufficient mixing to the free troposphere in our model. This could party be a 'signal-to-noise' problem; mixing from the PBL will leave only a small imprint on the large free tropospheric reservoir, where vertical profiles of SF_6 have a reasonably large standard deviation. However, if an additional 19% of SF_6 in the NH PBL would escape to the free troposphere and mix completely, abundances there would be impacted by about 3%, or ~0.15 ppt. Such a signal would be obvious in our measurements. This suggests that SF_6 should not only escape from the NH BL to the free troposphere, but also to the SH. Budget analysis indicates that our enhanced PBL mixing scheme slightly decreases the interhemispheric exchange by extracting SF_6 from the southerly branch of the Hadley circulation at the surface in the NH. This causes less SF_6 to leak to the SH in the tropics and does not contribute to a reduced meriodional gradient through this mechanism.

[53] Although the sensitivity to the strength of convection was not large enough to explain the mismatch in the meridional gradient, it was larger than that from vertical diffusion. Increased convection leads to a more vigorous Hadley circulation in the tropics and this increases the SF_6 flux from the NH to the SH. Convection is notoriously oversimplified in global transport models. A discussion of commonly used parameterizations and their shortcomings can be found in *Mahowald et al.* [1995]. In the near future, TM5 will use the convective fluxes from the ECMWF model directly, instead of calculating its own. Although first tests indicate that the changes are minor [*Olivie et al.*, 2004], further research is likely to bring improvements in the representation of convection. Such improvements should be tested against SF_6 to ensure a better agreement of the meridional gradients. Finally, analysis of the fluxes of SF_6 in our model also showed that ~10% of the yearly emissions eventually end up in the stratosphere. The exchange with the stratosphere in each hemisphere could contribute to meridional gradients, and introduce seasonal signals in free tropospheric SF_6. Exchange with this reservoir is not quantified very well though, and measurements to accurately describe the stratospheric SF_6 distribution do not exist. This is another uncertain factor influencing north-south gradients.

[54] Naturally, the sources of SF_6 are not known perfectly, and this could partly explain the reported biases. Currently, the meridional gradient of SF_6 is dominated by emissions from three regions (as defined by the TransCom regions in *Gurney et al.* [2002]): temperate North America (53%), temperate Asia (21%) and Europe (18%). Table 2 shows that the gap between bottom-up estimates and estimates from atmospheric data can be as large as 10%. This gap is always in the form of an underestimate by bottom-up estimates; for example, 500×10^3kg of SF_6 emissions are needed during 2000 to bring agreement. In our simple

approach, this is added by increasing all SF_6 emissions by 10%. In comparison, the extensive emission study of *Maiss and Brenninkmeijer* [1998], and the independent atmospheric study by *Bakwin et al.* [1997], suggest these emissions should be attributed partly to the annual refill of leaking insulators in power production/distribution (all three regions), and partly to the production of electrical equipment (mainly Asia and Europe). Uncertainties in SF_6 estimates arise due to the banking of purchased SF_6 for later use, uncertainties in the refill rates per region, and incomplete or missing data on some sources (military/space applications, specific industrial production and consumption activities in Russia/China). Selectively adding SF_6 emissions (500×10^3kg) to the NH subtropical regions showed only minor influence on the meridional gradient, since any additional SF_6 emission will have the largest impact on SF_6 concentrations on the hemisphere of origin. Shifting emissions from NH mid-latitudes to NH tropics (500×10^3kg) decreased the meridional gradient slightly as more SF_6 ended up in the NH free troposphere. However, the response was much too weak to explain the 19% mismatch in the meridional gradient. Uncertainty in the SF_6 distribution and magnitude in the NH is therefore not likely to explain this discrepancy.

[55] The largest differences between the TransCom models were seen in their vertical SF_6 distributions, but the observed vertical SF_6 profiles show only weak gradients and high variability, which means a longer measurement record might be needed to see statistically significant deviations for some models. It should nevertheless be possible to falsify some of these models by comparison to the data presented in this work, and thus reduce the uncertainty in the global CO_2 flux estimates as presented in *Gurney et al.* [2002]. Specifically, the 'within-model' variability will likely decrease by excluding models that perform poorly on SF_6. Repeating the TransCom exercises with these models is highly recommended because it will allow a better characterization of the seasonal rectifier and fossil fuel CO_2 gradients and thus identify biases in our current CO_2 flux estimates.

11. Conclusions

[56] The work presented here is an elaborate assessment of TM5's ability to reproduce transport, and we finally want to return to our original research questions (Section 1). Biases and errors (question 1) are discussed extensively in the previous sections. Here, we want to stress that despite some problems we diagnosed, TM5 performs very well on many aspects of global and regional transport, and it can be expected to grasp many of the relevant signals in CO_2. As a state-of-the-art global transport model, it performs as well as any other global model and offers the additional functionality and performance of a fine-scale, regional model. Regional nesting improves model performance in specific situations (question 2), but it also warrants close examination of local conditions for each site. We recommend careful study of local conditions for each new site introduced in a study, especially for sites on the continents. Horizontal grid refinement does not deteriorate (nor improve) the modeled large-scale SF_6 distribution, but it does add to our ability to reproduce variability at continental sites. Furthermore, it will allow us to derive the heterogeneous CO_2 fluxes at finer spatial scales and potentially decrease aggregation errors for the dense network planned in the North American Carbon Program.

[57] We have demonstrated some shortcomings and uncertainties of vertical transport in the PBL, and global exchange between northern and southern hemisphere that are likely shared by many global models used to estimate fluxes of CO_2. We want to stress that such uncertainties seriously limit our confidence in the results from inversions and will introduce biases in these estimates (question 3). The only way to address this problem is through continued careful validation with high quality measurements and continued intercomparison of these models such as done in the TransCom project. With many new continental, high-frequency sites being added in Europe and the US, improved subgrid scale parameterizations for these models are urgently needed.

[58] **Acknowledgments.** We would like to thank Pat Lang, Brad Hall, and Elaine Gottlieb for their indispensable role in assuring the high-quality of measurements presented here. We are grateful to Adam Hirsch and Anna Michalak for comments on the manuscript. We thank Jos Olivier for the bottom-up emission estimates. Computing facilities were provided by the 'Stichting Nationale Computer Faciliteiten' (NCF). Maarten Krol was supported by the PHOENICS project.

References

Bakwin, P. S., D. F. Hurst, P. P. Tans, and J. W. Elkins (1997), Anthropogenic sources of halocarbons, sulfur hexafluoride, carbon monoxide, and methane in the southeastern United States, *J. Geophys. Res.*, *102*(D13), 15,915–15,925.

Bergamaschi, P., F. Dentener, and M. Krol (2003), Inverse modelling of CH4 using an atmospheric zoom model, *Tech. Rep. EUR Rep. 21099 EN*, Joint Res. Cent., Ispra, Italy.

Berkvens, P. J. F., M. A. Botchev, J. G. Verwer, M. C. Krol, and W. Peters (2000), Solving vertical transport and chemistry in air pollution models, *Tech. Rep. MAS-R0023*, Cent. voor Wiskunde en Inf., Amsterdam, Netherlands.

Bousquet, P., P. Peylin, P. Ciais, C. Le Quere, P. Friedlingstein, and P. P. Tans (2000), Regional changes in carbon dioxide fluxes of land and oceans since 1980, *Science*, *290*(5495), 1342–1346.

Bregman, B., A. Segers, M. Krol, E. Meijer, and P. van Velthoven (2003), On the use of mass-conserving wind fields in chemistry-transport models, *Atmos. Chem. Phys.*, *3*, 447–457.

Chen, B. Z., J. M. Chen, J. Liu, D. Chan, K. Higuchi, and A. Shashkov (2004), A vertical diffusion scheme to estimate the atmospheric rectifier effect, *J. Geophys. Res.*, *109*, D04306, doi:10.1029/2003JD003925.

Ciais, P., P. P. Tans, M. Trolier, J. W. C. White, and R. J. Francey (1995), A large northern-hemisphere terrestrial CO_2 sink indicated by the C-13/C-12 ratio of atmospheric CO_2, *Science*, *269*(5227), 1098–1102.

Dargaville, R. J., R. M. Law, and F. Pribac (2000), Implications of interannual variability in atmospheric circulation on modeled CO_2 concentrations and source estimates, *Global Biogeochem. Cycles*, *14*(3), 931–943.

Denning, A. S., I. Y. Fung, and D. Randall (1995), Latitudinal gradient of atmospheric CO_2 due to seasonal exchange with land biota, *Nature*, *376*(6537), 240–243.

Denning, A. S., et al. (1999), Three-dimensional transport and concentration of SF6 - A model intercomparison study (TransCom 2), *Tellus, Ser. B*, *51*(2), 266–297.

Dentener, F., J. Feichter, and A. Jeuken (1999), Simulation of the transport of Rn-222 using on-line and off-line global models at different horizontal resolutions: A detailed comparison with measurements, *Tellus, Ser. B*, *51*(3), 573–602.

Dentener, F., W. Peters, M. Krol, M. van Weele, P. Bergamaschi, and J. Lelieveld (2003), Interannual variability and trend of CH4 lifetime as a measure for OH changes in the 1979–1993 time period, *J. Geophys. Res.*, *108*(D15), 4442, doi:10.1029/2002JD002916.

Dlugokencky, E. J., L. P. Steele, P. M. Lang, and K. A. Masarie (1994), The growth-rate and distribution of atmospheric methane, *J. Geophys. Res.*, *99*(D8), 17,021–17,043.

Enting, I. G., and J. V. Mansbridge (1989), Seasonal sources and sinks of atmospheric CO2: Direct inversion of filtered data, *Tellus, Ser. B*, *41*, 111–126.

Fan, S., M. Gloor, J. Mahlman, S. Pacala, J. Sarmiento, T. Takahashi, and P. Tans (1998), A large terrestrial carbon sink in North America implied by atmospheric and oceanic carbon dioxide data and models, *Science*, *282*(5388), 442–446.

Geller, L. S., J. W. Elkins, J. M. Lobert, A. D. Clarke, D. F. Hurst, J. H. Butler, and R. C. Myers (1997), Tropospheric SF_6: Observed latitudinal distribution and trends, derived emissions and interhemispheric exchange time, *Geophys. Res. Lett.*, *24*(6), 675–678.

Gurney, K. R., et al. (2002), Towards robust regional estimates of CO_2 sources and sinks using atmospheric transport models, *Nature*, *415*(6872), 626–630.

Gurney, K. R., et al. (2003), TransCom 3 CO_2 inversion intercomparison: 1. Annual mean control results and sensitivity to transport and prior flux information, *Tellus, Ser. B*, *55*(2), 555–579.

Heimann, M. (1995), The Global Atmospheric Tracer Model TM2 (model description and user manual), *Tech. Rep. 10*, Dtsch. Klimarechenzentrum, Hamburg, Germany.

Heimann, M., and C. D. Keeling (1989), A three-dimensional model of atmopsheric CO_2 transport based on observed winds: 2. Model description and simulated tracer experiments, in *Aspects of Climate Variability in the Pacific and Western Americas*, *Geophyis. Monogr. Ser.*, vol. 55, edited by D. H. Peterson, pp. 237–275, AGU, Washington, D. C.

Holtslag, A. A. M., and B. A. Boville (1993), Local versus nonlocal boundary-layer diffusion in a global climate model, *J. Clim.*, *6*(10), 1825–1842.

Houweling, S., F. Dentener, and J. Lelieveld (1998), The impact of nonmethane hydrocarbon compounds on tropospheric photochemistry, *J. Geophys. Res.*, *103*(D9), 10,673–10,696.

Jeuken, A., J. P. Veefkind, F. Dentener, S. Metzger, and C. R. Gonzalez (2001), Simulation of the aerosol optical depth over Europe for August 1997 and a comparison with observations, *J. Geophys. Res.*, *106*(D22), 28,295–28,311.

Jonson, J. E., J. K. Sundet, and L. Tarrason (2001), Model calculations of present and future levels of ozone and ozone precursors with a global and a regional model, *Atmos. Environ.*, *35*, 525–537.

King, D., and R. Schnell (2002), Summary report 2000–2001, vol. 26, edited by R. Rosson and C. Sweet, pp. 118–119, Natl. Oceanic and Atmos. Admin., Boulder, Colo.

Krol, M., W. Peters, P. J. F. Berkvens, and M. A. Botchev (2001), A new algorithm for two-way nesting in global models: Principles and applications, in *Proceedings of the 2nd International Conference on Air Pollution Modeling and Simulation*, edited by B. Sportisse, Springer Geosci., New York.

Krol, M., J. Lelieveld, D. E. Oram, G. A. Sturrock, S. A. Penkett, C. A. M. Brenninkmeijer, V. Gros, J. Williams, and H. A. Scheeren (2003), Continuing emissions of methyl chloroform from Europe, *Nature*, *421*(6919), 131–135.

Krol, M., S. Houweling, B. Bregman, M. v. d. Broek, A. Segers, P. v. Velthoven, W. Peters, F. Dentener, and P. Bergamaschi (2004), TM5, a global two-way nested chemistry-transport zoom model: Algorithm and Applications, *Atmos. Chem. Phys.*, in press.

Law, R. (1996), The selection of model-generated CO_2 data: A case study with seasonal biospheric sources, *Tellus, Ser. B*, *48*(4), 474–486.

Law, R. M., P. J. Rayner, L. P. Steele, and I. G. Enting (2003), Data and modelling requirements for CO_2 inversions using high-frequency data, *Tellus, Ser. B*, *55*(2), 512–521.

Levin, I., and V. Hesshaimer (1996), Refining of atmospheric transport model entries by the globally observed passive tracer distributions of (85)krypton and sulfur hexafluoride (SF6), *J. Geophys. Res.*, *101*(D11), 16,745–16,755.

Louis, J. F. (1979), A parametric model of vertical eddy fluxes in the atmosphere, *Boundary Layer Meteorol.*, *17*, 178–202.

Mahowald, N. M., P. J. Rasch, and R. G. Prinn (1995), Cumulus parameterizations in chemical transport models, *J. Geophys. Res.*, *100*(D12), 26,173–26,189.

Maiss, M., and C. A. M. Brenninkmeijer (1998), Atmospheric SF6: Trends, sources, and prospects, *Environ. Sci. Technol.*, *32*(20), 3077–3086.

Masarie, K. A., and P. P. Tans (1995), Extension and integration of atmospheric carbon-dioxide data into a globally consistent measurement record, *J. Geophys. Res.*, *100*(D6), 11,593–11,610.

Olivie, D. J. L., P. F. J. van Velthoven, A. C. M. Beljaars, and H. M. Kelder (2004), Comparison between archived and off-line diagnosed convective mass fluxes in the chemistry transport model TM3, *J. Geophys. Res.*, *109*, D11303, doi:10.1029/2003JD004036.

Olivier, J., and J. Berdowski (2001), Global emissions sources and sinks, in *The Climate System*, edited by J. Berdowski, R. Guicherit, and B. Heij, pp. 33–78, A. A. Balkema, Brookfield, Vt.

Peters, W., M. Krol, F. Dentener, and J. Lelieveld (2001), Identification of an El Nino-Southern Oscillation signal in a multiyear global simulation of tropospheric ozone, *J. Geophys. Res.*, *106*(D10), 10,389–10,402.

Prinn, R. G., R. A. Rasmussen, P. G. Simmonds, F. N. Alyea, D. M. Cunnold, B. C. Lane, C. A. Cardelino, and A. J. Crawford (1983), The Atmospheric Lifetime Experiment: 5. Results for CH3CCl3 based on three years of data, *J. Geophys. Res.*, *88*, 8415–8426.

Randerson, J. T., M. V. Thompson, T. J. Conway, I. Y. Fung, and C. B. Field (1997), The contribution of terrestrial sources and sinks to trends in the seasonal cycle of atmospheric carbon dioxide, *Global Biogeochem. Cycles*, *11*(4), 535–560.

Ravishankara, A. R., S. Solomon, A. A. Turnipseed, and R. F. Warren (1993), Atmospheric lifetimes of long-lived halogenated species, *Science*, *259*(5092), 194–199.

Rodenbeck, C., S. Houweling, M. Gloor, and M. Heimann (2003), Time-dependent atmospheric CO_2 inversions based on interannually varying tracer transport, *Tellus, Ser. B*, *55*(2), 488–497.

Russel, G., and J. Lerner (1981), A new finite-differencing scheme for the tracer transport equation, *J. Appl. Meteorol.*, *20*, 1483–1498.

Segers, A., P. van Velthoven, B. Bregman, and M. Krol (2002), On the computation of mass fluxes for Eulerian transport models from spectral meteorological fields, in *Computational Science - ICCS 2002: International Conference, Lecture Notes in Computer Science*, vol. 2330, edited by P. Sloot et al., pp. 767–776, Springer-Verlag, New York.

Taghavi, M., S. Cautenet, and G. Foret (2003), Simulation of ozone production in a complex circulation regime using nested grids, *Atmos. Chem. Phys. Discuss.*, *3*, 3833–3867.

Tang, Y. (2002), A case study of nesting simulation for the Southern Oxidants Study 1999 at Nashville, *Atmos. Environ.*, *36*, 1691–1704.

Tans, P. P., I. Y. Fung, and T. Takahashi (1990), Observational constraints on the global atmospheric CO_2 budget, *Science*, *247*(4949), 1431–1438.

Thoning, K. W., P. P. Tans, and W. D. Komhyr (1989), Atmospheric carbon-dioxide at Mauna Loa observatory: 2. Analysis of the NOAA GMCC data, 1974–1985, *J. Geophys. Res.*, *94*(D6), 8549–8565.

Tiedtke, M. (1993), Representation of clouds in large-scale models, *Mon. Weather Rev.*, *121*(11), 3040–3061.

van den Broek, M. M. P., et al. (2003), The impact of model grid zooming on tracer transport in the 1999/2000 Arctic polar vortex, *Atmos. Chem. Phys.*, *3*, 1833–1847.

Wofsy, S., and R. Harriss (2002), The North American Carbon Program (NACP), technical report, U.S. Global Change Res. Program, NACP Comm. U.S. Interagency Carbon Cycle Sci. Program.

P. Bergamaschi and F. J. Dentener, Joint Research Centre (JRC), I-21020 Ispra, Italy.

L. Bruhwiler, E. J. Dlugokencky, G. Dutton, J. B. Miller, W. Peters, and P. P. Tans, Climate Monitoring and Diagnostics Laboratory, NOAA, 325 Broadway R/CMDL-1, Boulder, CO 80302, USA. (wouter.peters@noaa.gov)

M. C. Krol, Institute for Marine and Atmospheric Research Utrecht (IMAU), 3584 Utrecht, Netherlands.

P. v. Velthoven, Royal Netherlands Meteorological Institute (KNMI), 3730 De Bilt, Netherlands.